Sparse Radar Waveform Design Exploiting Consecutive Integer Set Partitioning

Md. Waqeeb T. S. Chowdhury [†], Yimin D. Zhang [†], and Braham Himed [‡]

[†] Department of Electrical and Computer Engineering, Temple University, Philadelphia, PA 19122, USA
[‡] Distributed RF Sensing Branch, Air Force Research Laboratory, WPAFB, OH 45433, USA

***Abstract*—In this paper, we exploit the concept of identical partitioning of an integer set to support orthogonal radar waveforms with non-overlapping slow-time pulses. The set of slow-time pulses in a coherent processing interval (CPI) is partitioned into multiple identical subsets, and each subset is used to design sparse slow-time pulses for a single radar with low lag redundancy. Such waveform design based on integer set partitioning not only allows co-existence of multiple radars over a particular CPI, but also ensures that each radar unit can enjoy an extended dwell time, thereby maintaining a high-resolution estimation of the target Doppler frequencies. A modified difference co-chirp-based approach is exploited for range-Doppler estimation of targets with a low computational complexity.**

Keywords: Integer set partitioning, sparse waveform design, difference co-chirp, consecutive lag, sparse sampling.

I. Introduction

Sparse modeling in the context of sensor arrays [1–6] and radar waveform design [7–10] has attracted considerable interests and made significant advancements recently. This progress is driven primarily by the benefits of sparsity-based signal sampling and processing in enhancing the sensing capabilities and accuracy, as well as optimizing the utilization of resources [11–16]. The adoption of sparse sampling methods in waveform design is becoming increasingly popular due to the strong demands for high-resolution sensing and the availability of sparse reconstruction methods. There is a growing interest in designing sparse waveforms that enable multiple radars to make effective use of the time and spectrum resources. For instance, random sparse step-frequency waveforms are considered in [8, 10] to select a subset of step frequencies in a step-frequency radar. By exploiting only a subset of the available step frequencies, it becomes feasible to allow multiple radars to operate simultaneously while sharing the same spectrum band. An analogous approach proposed in [17–19] introduces sparsity in slow time by incorporating radar waveforms with non-uniform pulse repetition intervals (PRIs).

While such approaches have explored sparse waveform design and its application to high-resolution target sensing, investigation of jointly designing multiple sparse radar waveform sets for resource sharing across multiple radar systems is lacking. Recently, identical partitioning of a consecutive integer set into two non-overlapping subsets was proposed in [20]. Such partitioning strategies are developed based on the nested structure in order to provide a high number of consecutive lags and low lag redundancy as compared to localized counterparts. The prototype nested partitioning method was further extended to super-nested partitioning schemes which provide 2^G identical subsets for some integer $G \geq 1$. Such partitioning strategies can be generalized to more flexible integer set divisions [21].

In this paper, we consider the co-design of multiple slow-time radar waveforms following the super-nested partition scheme developed in [20]. The slow-time indices along a CPI are treated as a consecutive integer set that is partitioned into multiple identical subsets such that each subset of slow-time pulses is used for target Doppler estimation in radar. Such waveform design motivated by the partitioning concept offers sparse radar waveform design that allows for multiple radars to co-exist with effective utilization of sparse slow-time pulses. Different super-nested partitioning approaches are examined to provide effective solutions. It is noted that, since the sparsely partitioned waveforms achieve consecutive lags, existing methods developed for difference co-chirp-based range-Doppler estimation for non-uniform PRI radars, such as that reported in [19], can be exploited. Nevertheless, compared to such existing methods which exploit the entire fast-time data for lag computation, they are modified to provide fast computation with enhanced performance.

Notations: We use bold lower-case (upper-case) characters to represent vectors (matrices). Notations $(\cdot)^*$, $(\cdot)^{\mathrm{T}}$, and $(\cdot)^{\mathrm{H}}$ denote complex conjugation, transpose, and Hermitian operations, respectively. $\mathrm{diag}(\cdot)$ constructs a diagonal matrix and $\circledast$ represents the convolution operation. $\otimes$ and $\circ$ respectively denote the Kronecker and element-wise products, and $\jmath = \sqrt{-1}$ denotes the unit imaginary number. Furthermore, $\{0,1\}^{M\times N}$ and $\mathbb{C}^{M\times N}$ stand for the $M \times N$ binary and complex spaces, respectively.

II. System Model

A. Radar Signal Model

We consider pulse radar signals exploiting linear frequency-modulated (LFM) waveforms. Denote T_{pri} and T_{pw} as the PRI and the duration of the transmitted pulse, respectively, and $\delta = T_{\mathrm{pw}}/T_{\mathrm{pri}} \ll 1$ is the duty cycle of the transmit radar waveform. When the carrier frequency is f_c and the signal

This material is based upon work supported by the Air Force Office of Scientific Research under award number FA9550-23-1-0255. Any opinions, findings, and conclusions or recommendations expressed in this material are those of the authors and do not necessarily reflect the views of the United States Air Force.

bandwidth is B, the transmit LFM waveform of the nth pulse is given as

$$s(n,t) = \Pi_n \cdot e^{\jmath 2\pi \left[f_c(t-nT_{\rm pri}) + \frac{\beta(t-nT_{\rm pri})^2}{2} \right]}, \quad (1)$$

where t is the fast time, $\beta = B/T_{\rm pw}$ is the chirp rate, and

$$\Pi_n = \text{rect}\left(\frac{t-nT_{\rm pri}}{T_{\rm pw}}\right) = \begin{cases} 1, & nT_{\rm pri} \le t \le nT_{\rm pri} + T_{\rm pw}, \\ 0, & \text{otherwise} \end{cases} \quad (2)$$

is a rectangular pulse window. The maximum unambiguous range of the radar is given by

$$R_{\max} = \frac{cT_{\rm pri}}{2} = \frac{c}{2f_{\rm pri}}, \quad (3)$$

where $f_{\rm pri} = 1/T_{\rm pri}$ denotes the pulse repetition frequency (PRF) and c is the propagation velocity of electromagnetic waves.

Assuming P uncorrelated targets in the radar's field of view, the signal received at the radar is the weighted sum of $s(n,t)$ with delays reflecting the target range, given as

$$y(n,t) = \sum_{p=1}^{P} y_p(n,t) = \sum_{p=1}^{P} \alpha_p s(n, t-\tau_p), \quad (4)$$

where α_p and τ_p respectively denote the reflectivity and the round-trip time delay of the pth target. Applying pulse compression, the beat signal is obtained by correlating the received signal and the transmit signal $s(n,t)$, expressed as

$$x'(n,t) = s^*(n,t) \circledast y(n,t) = \int_0^{T_{\rm pri}} y(n,\tau) s^*(n, t-\tau)\, \mathrm{d}\tau. \quad (5)$$

Passing the beat signal through a low-pass filter yields $x(n,t) = \sum_{p=1}^{P} x_p(n,t)$, where the phase term of $x_p(n,t)$ is given as

$$\phi_p(n,t) = 2\pi \left[f_c \tau_p(n,t) - \beta t \tau_p(n,t) + 0.5\beta \tau_p^2(n,t) \right], \quad (6)$$

$\tau_p(n,t) = 2(R_{p0} + v_p n T_{\rm pri} + v_p t)/c$ is the round-trip delay, and R_{p0} denotes the initial range of the pth target.

Ignoring the higher-order terms of t, the beat frequency of the pth target can be expressed as

$$f_b^p = f_R^p + f_v^p = \frac{2BR_p}{cT_{\rm pw}} + \frac{2f_c v_p}{c}, \quad (7)$$

where $f_R^p = 2BR_p/(cT_{\rm pw})$ and $f_v^p = 2f_c v_p/c$ are, respectively, the beat frequency components corresponding to the pth target due to range and Doppler shift.

Given the maximum unambiguous range of $R_{\max}$, the maximum beat frequency due to the target range is given as $f_{\max}^b = 2\beta R_{\max}/c$. In order to avoid under-sampling of the beat signal, the sampling interval T_s of the beat signal should be chosen such that $T_s^{-1} \ge 2f_{\max}^b$. In this case, the ith fast-time sample in the nth pulse of the beat signal becomes (we use the same notation x without confusion)

$$x(n,i) = \sum_{p=1}^{P} e^{\jmath 2\pi \left(f_R^p i T_s + f_v^p n T_{\rm pri} \right)}. \quad (8)$$

When all slow-time pulses are present, the range and Doppler information of the targets can be obtained by applying the fast Fourier transform (FFT) along the fast-time and slow-time samples of $x(n,i)$, $n = 0, \cdots, N_d - 1$ and $i = 0, \cdots, N_r - 1$. However, in the underlying problem, we use a sparse subset of slow-time pulses in each radar. To avoid high sidelobes in the Doppler estimation, we use co-chirp-based processing as discussed in Section III.

B. Sparse Waveform Design by Partitioning

In this subsection, we summarize the identical partitioning approaches developed in [20] for a one-dimensional (1-D) and two-dimensional (2-D) consecutive sets of integers. The nested partitioning scheme is exploited, which is shown to provide subsets with more consecutive lags and lower redundancy compared to the localized partitioning scheme.

The general rule for partitioning a 1-D integer set into two nested subsets is that any consecutive integer set consisting of an even number of M elements can be identically partitioned into two nested subsets such that each nested subset contains 2 inner elements and $N = M/2 - 2$ outer elements. An example is shown in Fig. 1(a) for $M = 12$, i.e., $N = 4$, where the two colors indicate two partitioned subsets. Each subset consists of 6 nested elements with 2 inner elements and 4 outer elements, and yields consecutive lags between -9 and 9. The two subarrays share the same weight function of the difference lags as shown in Fig. 1(b).

The elements of the first and the second nested subsets are respectively given as

$$\mathbb{Q}_1 = \{1, 2, 4 : 2 : 2N+2\}, \quad (9)$$

$$\mathbb{Q}_2 = \{3 : 2 : 2N+1, 2N+3, 2N+4\}. \quad (10)$$

We define masking vectors $\mathbf{b}_g \in \{0,1\}^{M\times 1}$ for these two subsets $g \in \{1,2\}$ as

$$\mathbf{b}_g(k) = \begin{cases} 1, & k \in \mathbb{Q}_g, \\ 0, & k \notin \mathbb{Q}_g. \end{cases} \quad (11)$$

The nested partitioning scheme discussed above only constructs $g = 2$ subsets. To construct $g = 2^G$ subsets for integer $G \ge 2$, the super-nested partitioning scheme is adopted [20]. We first extend the 1-D nested partitioning scheme into a 2-D problem in which the above-mentioned 1-D nested partitioning is applied to each of the two dimensions of a 2-D consecutive integer set. Similar to the 1-D case, we define $M^{[1]} = 2N^{[1]} + 4$ and $M^{[2]} = 2N^{[2]} + 4$ as the numbers of elements in both dimensions, where $N^{[1]}$ and $N^{[2]}$ are the numbers of outer groups of the nested structure along the two dimensions. The corresponding masking vectors are denoted as $\mathbf{b}_{g_1}^{[1]} \in \{0,1\}^{M^{[1]}\times 1}$ and $\mathbf{b}_{g_2}^{[2]} \in \{0,1\}^{M^{[2]}\times 1}$, respectively, for $g_1, g_2 \in \{1,2\}$. Then, the masking matrix for the 2-D partition $\mathbf{B}_{g_1 g_2} \in \{0,1\}^{M^{[1]}\times M^{[2]}}$ can be obtained as

$$\mathbf{B}_{g_1 g_2} = \mathbf{b}_{g_1}^{[1]} \left(\mathbf{b}_{g_2}^{[2]} \right)^{\rm T}. \quad (12)$$

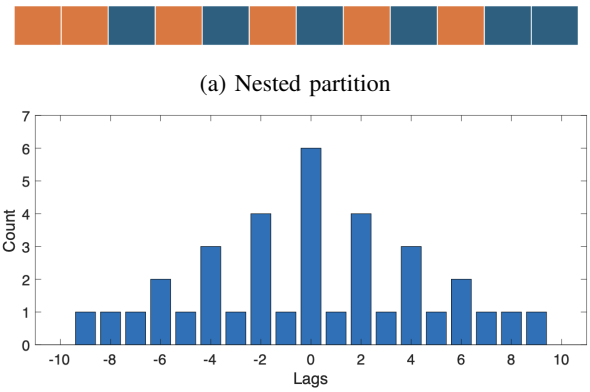

(a) Nested partition

(b) Weight function of difference lags of the nested subsets

Fig. 1: Two-subset nested partitioning of a 12-element consecutive integer set and the weight function of difference lags.

Note that, in this case, $G = 2$ and thus $2^G = 4$ identical subsets are obtained from the 2-D integer set.

To derive the super-nested partitioning appoach, the 2-D masking matrix $\mathbf{B}$ is vectorized to obtain the masking vector of the 1-D super-nested partitioning scheme, rendering four 1-D identical subsets. Depending on the direction of vectorization, the mask vector can take one of the following two options:

$$\tilde{\mathbf{b}}^{[a]}_{g_1g_2} = \mathrm{vec}(\mathbf{B}_{g_1g_2}) = \mathbf{b}^{[1]}_{g_1} \otimes \mathbf{b}^{[2]}_{g_2}, \tag{13}$$

$$\tilde{\mathbf{b}}^{[b]}_{g_1g_2} = \mathrm{vec}(\mathbf{B}^{\mathrm{T}}_{g_1g_2}) = \mathbf{b}^{[2]}_{g_2} \otimes \mathbf{b}^{[1]}_{g_1}. \tag{14}$$

It is clear that $\tilde{\mathbf{b}}^{[a]}_{g_1g_2}$ and $\tilde{\mathbf{b}}^{[b]}_{g_1g_2}$ are identical when $M^{[1]} = M^{[2]}$. On the other hand, when $M^{[1]} \neq M^{[2]}$, these two options render different partitioning patterns.

Fig. 2(a) shows an example of four 2-D nested partitions for the case of $M^{[1]} = 12$ and $M^{[2]} = 16$. The numbers of outer groups in the two dimensions are respectively $N^{[1]} = 4$ and $N^{[2]} = 6$. Figs. 2(b) and 2(c) show the two super-nested structures that are obtained by vectorizing the first 2-D nested partition pattern, shown in Fig. 2(a), in different ways respectively corresponding to $\tilde{\mathbf{b}}^{[a]}_{11}$ and $\tilde{\mathbf{b}}^{[b]}_{11}$. It is clear that the super-nested partition pattern depicting in Fig. 2(b) renders a higher number of $(2N^{[1]}+4)(2N^{[2]}+1)+(2N^{[1]}+1) = 165$ consecutive lags, compared to the one shown in Fig. 2(b) which generates $(2N^{[1]}+1)(2N^{[2]}+4)+(2N^{[2]}+1) = 158$ consecutive lags. Therefore, the former is a preferred choice and will be adopted in the sequel.

III. Range-Doppler Estimation using Super-Nested Radar Waveform

In this section, we elaborate on the range-Doppler estimation of targets using pulsed radar waveforms that are sparse along the slow time. The indexes of slow-time pulses over a CPI is considered as a consecutive integer set that is partitioned to multiple identical subsets following the super-nested partitioning scheme. Note that such radar waveforms with sparsity along the slow time cannot be effectively used by performing

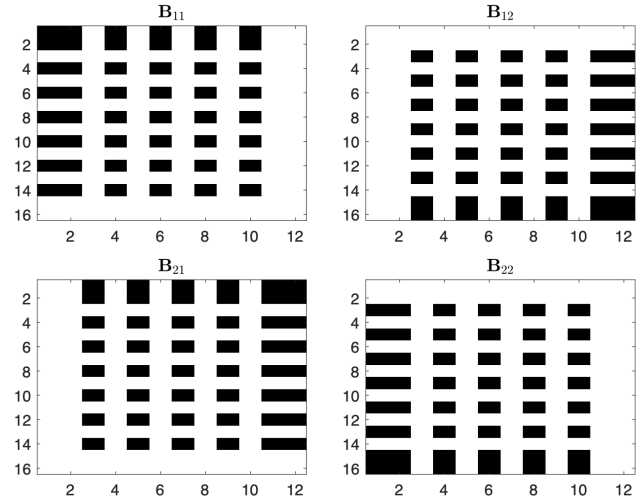

(a) Masking matrices of four partitions from a 2-D integer set

(b) Super-nested partition masking vector $\tilde{\mathbf{b}}^{[a]}_{11} = \mathrm{vec}(\mathbf{B}_{11})$

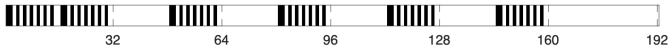

(c) Super-nested partition masking vector $\tilde{\mathbf{b}}^{[b]}_{11} = \mathrm{vec}(\mathbf{B}^{\mathrm{T}}_{11})$

Fig. 2: Two possible super-nested partitions from a 2-D nested partition when $M^{[1]} = 12$ and $M^{[2]} = 16$.

direct FFT for unambiguous Doppler estimation due to the presence of high sidelobes. Since super-nested partitions yield consecutive difference lags, difference co-chirp-based range-Doppler estimation for non-uniform PRI radars proposed in [19] can be exploited for such radar waveforms.

Co-chirp-based processing exploits co-chirp lags instead of the raw slow-time data for target Doppler estimation. By exploiting fast-time data samples for the computation of a second-order covariance matrices, we can obtain consecutive slow-time lags from the sparse super-nested pulses.

Denote $\tilde{\mathbf{x}}(i) = [x(0,i), \cdots, x(N_d-1,i)]^{\mathrm{T}}$ as the slow-time data vector corresponding to the ith fast-time sample for $i = 0, \cdots, N_r-1$, and $\tilde{\mathbf{x}}_{g_1g_2}(i) = \tilde{\mathbf{b}}^{[a]}_{g_1g_2} \circ \tilde{\mathbf{x}}(i)$ as that observed at the radar exploiting the g_1g_2th sparse super-nested slow-time subset with $g_1, g_2 \in \{1,2\}$. We can express $\tilde{\mathbf{x}}_{g_1g_2}(i)$ as

$$\tilde{\mathbf{x}}_{g_1g_2}(i) = \tilde{\mathbf{b}}^{[a]}_{g_1g_2} \circ [\mathbf{A}\boldsymbol{\Sigma}\mathbf{s}(i) + \mathbf{n}(i)], \tag{15}$$

where $\mathbf{A} = \left[\mathbf{a}(f_v^1), \mathbf{a}(f_v^2), \cdots, \mathbf{a}(f_v^P)\right]$ is the Doppler manifold with $\mathbf{a}(f_v^p) = [1, e^{\jmath 2\pi f_v^p T_{\mathrm{pri}}}, \cdots, e^{\jmath 2\pi f_v^p (N_d-1) T_{\mathrm{pri}}}]^{\mathrm{T}}$, $\boldsymbol{\Sigma} = \mathrm{diag}([\alpha_1, \cdots, \alpha_P])$, $\mathbf{s}(i) = [e^{\jmath 2\pi f_b^1 i T_s}, \cdots, e^{\jmath 2\pi f_b^P i T_s}]^{\mathrm{T}}$, and $\mathbf{n}(i)$ is the additive noise in the ith fast-time sample.

The co-chirp processing is similar to the one addressed in automotive radar applications [19] where frequency-modulated continuous-wave (FM-CW) waveforms are used to detect targets that are relatively close to the radar. For such con-

(a) Super-nested partition when $M^{[1]} = M^{[2]} = 16$

(b) Super-nested partition when $M^{[1]} = 32,\ M^{[2]} = 8$

(c) Alternate super-nested partition when $M^{[1]} = 32,\ M^{[2]} = 8$

Fig. 3: Super-nested partitioning of a 256-element integer set for different combinations of $M^{[1]}$ and $M^{[2]}$.

tinuous waveforms, the co-chirp lags are computed using all fast-time samples. On the other hand, for pulse radar waveforms considered in the underlying problem, particularly when the duty cycle is low, we modify the computation of the autocorrelation function such that it is computed based only on the fast-time data for the range cells where targets are detected in target range estimation. In so doing, we reduce the computational complexity while reducing the effect of noise as target-free fast-time samples are excluded. It is noted that, unlike [19] which requires range-Doppler association of the targets because the entire fast-time data are used for sample covariance computation and Doppler estimation, such association is not needed in the proposed approach because Doppler estimation is separately performed for each range cell.

Denote $\mathbb{N}_k$ as the fast-time samples that are associated with range cell k, the sample covariance matrix in the slow-time domain corresponding only to targets located at this range cell is estimated as

$$\mathbf{R} = \frac{1}{|\mathbb{N}_k|} \sum_{i \in \mathbb{N}_k} \tilde{\mathbf{x}}_{g_1 g_2}(i) \tilde{\mathbf{x}}^{\mathrm{H}}_{g_1 g_2}(i), \tag{16}$$

where $|\mathbb{N}_k| \ll N_r$ denotes the cardinality of $\mathbb{N}_k$ representing the number of fast-time samples corresponding to the kth range cell. As we discussed in Section II, such a covariance matrix provides consecutive slow-time lags between $-(2N^{[1]}+4)(2N^{[2]}+1)-(2N^{[1]}+1)$ and $(2N^{[1]}+4)(2N^{[2]}+1)+(2N^{[1]}+1)$, which can be used to estimate Doppler frequencies through an FFT for the range cell being considered.

IV. Simulation Results

We consider a pulsed radar with LFM waveforms with carrier frequency $f_c = 500$ MHz and bandwidth $B = 150$ MHz. The rendered maximum unambiguous range and velocities are $R_{\max} = 150$ km and $v_{\max} = 150$ m/s, respectively. The PRI and the pulse width of the waveform are assumed to be $T_{\mathrm{pri}} = 1$ ms and $T_{\mathrm{pw}} = 30$ μs with a duty cycle of $\delta = 3\%$. The number of fast-time samples in a slow-time slot is $N_r = 2^{20}$, and one CPI contains $N_d = 256$ slow-time pulses.

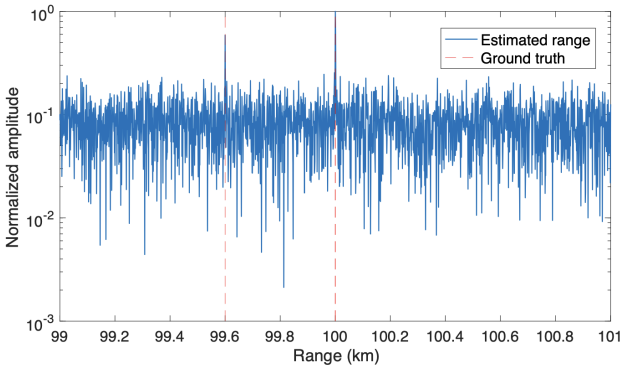

Fig. 4: Range spectrum from FFT along fast time.

We analyze two configurations to partition the slow-time slots. The first configuration assumes identical $M^{[1]} = M^{[2]} = 16$, i.e., $N^{[1]} = N^{[2]} = 6$, whereas in the second configuration, they take different values of $(M^{[1]}, M^{[2]}) = (32, 8)$ or $(N^{[1]}, N^{[2]}) = (14, 2)$. Since the 2-D partition obtained from the first configuration is symmetric, only one super-nested pattern can be obtained, as shown in Fig. 3(a). On the other hand, for the second configuration, since the 2-D nested partition is asymmetric, it is possible to obtain two super-nested partitions, respectively depicted in Figs. 3(b) and 3(c), with the former providing more consecutive lags. We compare both super-nested partitions depicted in Figs. 3(a) and 3(b) to design the sparse slow-time waveforms. The first super-nested subset with $g_1 = g_2 = 1$ is considered.

We consider three targets in the scene. Two targets are located at a range of 100 km with radial velocities of 100 m/s and 105 m/s, respectively, and another target is located at range 99.6 km with radial velocity 90 m/s. The input signal-to-noise ratio (SNR) evaluated at the beat signal is assumed to be -30 dB for all targets.

Fig. 4 shows the range estimates of the three targets by applying an FFT on the fast-time samples. The result show two peaks in the range where the 99.6 km range contains one target whereas two targets are included in range 100 km. The range-Doppler spectrum obtained by directly applying a 2D FFT on the sparse radar data is shown in Fig. 5(a). It produces high sidelobes along the Doppler direction due to the sparse slow-time pulses, making the identification challenging. On the other hand, the Doppler spectrum obtained from applying the FFT to the co-chirp lags corresponding to the 99.6 km and 100 km ranges produces clearly resolved estimates of the target velocities in both range cells. Figs. 5(b) and 5(c) show the Doppler estimates for the two super-nested patterns depicted in Figs. 3(a) and 3(b) with similar lags, and the results obtained from all consecutive slow-time pulses are also included for comparison. While the case of full slow-time pulses shows a slightly lower noise floor, these configurations result in similar performance, thus demonstrating the efficiency of sparse radar waveform design using the proposed partitioning methods.

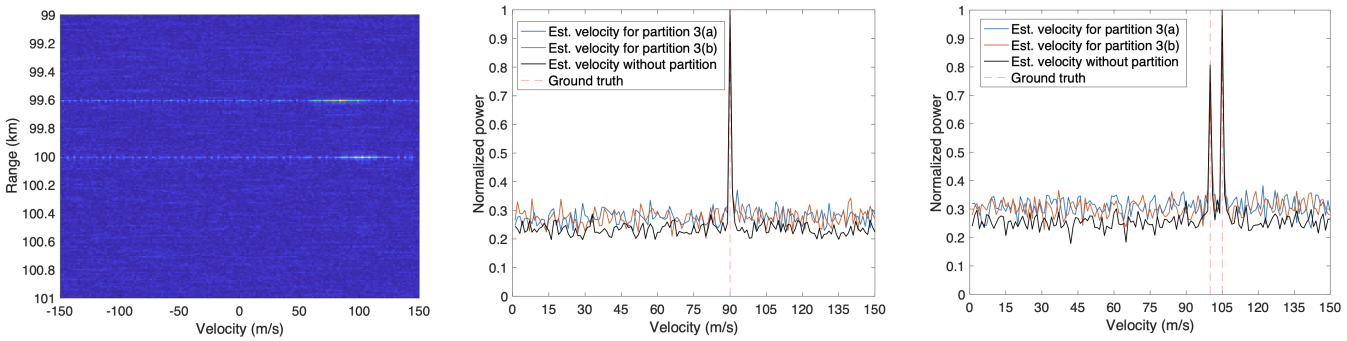

(a) 2D FFT on sparse radar data (b) Doppler estimate of target at 99.6 km (c) Doppler estimate of targets at 100 km

Fig. 5: Applying FFT on interpolated Doppler covariance matrix resolves target velocities without ambiguity.

V. Conclusion

In this paper, we applied the concept of partitioning a consecutive integer set to design multiple non-overlapping subsets of sparse slow-time pulses. Such partitioning allows for the total available CPI to be shared by multiple radar systems to simultaneously perform independent sensing without mutual interference. The super-nested partitioning was employed for sparse waveform design, and a modified difference co-chirp-based range-Doppler estimation technique was applied to successfully recover the Doppler information of the targets from the slow-time data corresponding to sparse radar pulses. Compared to the existing difference co-chirp-based approach utilizing the entire fast-time data, the proposed approach provides a computationally more effective solution with reduced noise effect and avoids the range-Doppler association issue.

VI. References

[1] P. Pal and P. P. Vaidyanathan, "Nested arrays: A novel approach to array processing with enhanced degrees of freedom," *IEEE Trans. Signal Process.*, vol. 58, no. 8, pp. 4167–4181, Aug. 2010.

[2] P. P. Vaidyanathan and P. Pal, "Sparse sensing with co-prime samplers and arrays," *IEEE Trans. Signal Process.*, vol. 59, no. 2, pp. 573–586, Feb. 2011.

[3] S. Qin, Y. D. Zhang, and M. G. Amin, "Generalized coprime array configurations for direction-of-arrival estimation," *IEEE Trans. Signal Process.*, vol. 63, no. 6, pp. 1377–1390, March 2015.

[4] J. Liu, Y. Zhang, Y. Lu, S. Ren, and S. Cao, "Augmented nested arrays with enhanced DOF and reduced mutual coupling," *IEEE Trans. Signal Process.*, vol. 65, no. 21, pp. 5549–5563, Nov. 2017.

[5] Z. Zheng, W. Wang, Y. Kong and Y. D. Zhang, "MISC array: A new sparse array design achieving increased degrees of freedom and reduced mutual coupling effect," *IEEE Trans. Signal Process.*, vol. 67, no. 7, pp. 1728–1741, April 2019.

[6] A. Ahmed and Y. D. Zhang, "Generalized non-redundant sparse array designs," *IEEE Trans. Signal Process.*, vol. 69, pp. 4580–4594, Aug. 2021.

[7] S. Na, K. V. Mishra, Y. Liu, Y. C. Eldar, and X. Wang, "TenDSuR: Tensor-based 4D sub Nyquist radar," *IEEE Signal Process. Lett.*, vol. 26, no. 2, pp. 237–241, 2018.

[8] K. V. Mishra, S. Mulleti, and Y. C. Eldar, "RaSSteR: Random sparse step-frequency radar," arXiv preprint arXiv: 2004.05720, 2020.

[9] W. P. Plessis, "Simultaneous unambiguous range and Doppler through non-uniform sampling," in *Proc. IEEE Radar Conf.*, Florence, Italy, Sept. 2020, pp. 1–6.

[10] S. Sun and Y. D. Zhang, "4D automotive radar sensing for autonomous vehicles: A sparsity-oriented approach," *IEEE Sel. Topics Signal Process.*, vol. 15, no. 4, pp. 879–891, June 2021.

[11] Z. M. Liu, Z. T. Huang and Y. Y. Zhou, "Array signal processing via sparsity-inducing representation of the array covariance matrix," *IEEE Trans. Aerosp. Electron. Syst.*, vol. 49, no. 3, pp. 1710–1724, July 2013.

[12] A. Liu, X. Zhang, Q. Yang, and W. Deng, "Fast DOA estimation algorithms for sparse uniform linear array with multiple integer frequencies," *IEEE Access*, vol. 6, pp. 29952–29965, May 2018.

[13] C. Zhou, Y. Gu, X. Fan, Z. Shi, G. Mao, and Y. D. Zhang, "Direction-of-arrival estimation for coprime array via virtual array interpolation," *IEEE Trans. Signal Process.*, vol. 66, no. 22, pp. 5956–5971, Nov. 2018.

[14] S. Zhang, A. Ahmed, Y. D. Zhang, and S. Sun, "Enhanced DOA estimation exploiting multi-frequency sparse array," *IEEE Trans. Signal Process.*, vol. 69, pp. 5935–5946, Oct. 2021.

[15] M. W. T. S. Chowdhury and Y. D. Zhang, "Unambiguous DOA estimation using multi-frequency rational sparse arrays," in *Proc. Asilomar Conf. Signals, Syst. Comput.*, Pacific Grove, CA, Oct. 2023.

[16] A. Ahmed and Y. D. Zhang, "Optimized resource allocation for distributed joint radar-communication system," *IEEE Trans. Veh. Technol.*, vol. 73, no. 3, pp. 3872–3885, March 2024.

[17] M. W. Maier, "Non-uniform PRI pulse-Doppler radar," in *Proc. Southeastern Symp. Systm Theory*, Tuscaloosa, AL, March 1993, pp. 164–168.

[18] J. Li and Z. Chen, "Research on random PRI PD radar target velocity estimate based on NUFFT," in *Proc. IEEE CIE Int. Conf. Radar*, Chengdu, China, Oct. 2011, pp. 1801–1803.

[19] L. Xu, S. Sun, K. V. Mishra, and Y. D. Zhang, "Automotive FMCW radar with difference co-chirps," *IEEE Trans. Aerosp. Electron. Syst.*, vol. 59, no. 6, pp. 8145–8165, Dec. 2023.

[20] Y. D. Zhang and S. Sun, "Identical partitioning of consecutive integer set," in *Proc. 2024 IEEE Sensor Array and Multich. Signal Process. Workshop*, Corvallis, OR, July 2024.

[21] A. Namboothiri, M. W. Chowdhury, and Y. D. Zhang, "Non-overlapping identical division of integer set," in *Proc. Asilomar Conf. Signals, Syst., Comput.*, Pacific Grove, CA, Oct. 2024.